

Subterahertz spectroscopy at He-3 temperatures

D. N. Basov,^{a)} S. V. Dordevic, E. J. Singley, W. J. Padilla, and K. Burch
Department of Physics, University of California San Diego, La Jolla, California 92093

J. E. Elenewski and L. H. Greene
Department of Physics and Fredrick Seitz Materials Research Laboratory, University of Illinois at Urbana-Champaign, Urbana, Illinois 61801

J. Morris and R. Schickling
Infrared Laboratories, 1808 E. 17th Street, Tucson, Arizona 85719-6505

(Received 26 November 2002; accepted 8 July 2003)

We report on the design and implementation of an instrument for spectroscopic studies of materials at sub-terahertz (THz) frequencies at temperatures down to 340 mK. We achieved consistent operation under these rather extreme conditions by coupling a modified Martin–Puplett interferometer to a single cryogenic unit housing two independently controlled He-3 platforms: one as a sample stage and the other for bolometric detectors. Both the optical scheme of the interferometer and detector layout are tailored for the use of the two-channel data acquisition mode which is especially advantageous for measurement of absolute values of reflectance as well as for high-resolution spectroscopy. We document the reliable performance of the sub-THz apparatus with several experiments exploring electrostatics of both conventional and high- T_c superconductors.

© 2003 American Institute of Physics. [DOI: 10.1063/1.1614855]

I. INTRODUCTION

Characteristic energy scales of a large variety of fundamentally important phenomena fall into the terahertz region: 100 GHz–3 THz (3–100 cm^{-1}). These include absorption bands of interstellar medium,¹ molecular vibrational modes, emission of hydroxyl radical (OH),² and many others. The terahertz (THz) range is equally important for technological applications involving aircraft ranging³ and guidance under zero visibility conditions,⁴ imaging systems,^{5–7} as well as noninvasive detection of plastic weapons or explosives.⁸ The terahertz range is exceptionally rich in terms of diverse effects in condensed matter physics that fall within this frequency interval. An incomplete list includes magnetic⁹ and cyclotron plasma¹⁰ resonances, localized lattice modes,¹¹ Josephson plasma modes¹² and energy gaps in superconductors,^{13,14} absorption structure of organic molecular magnets,^{15,16} response features of materials with strongly correlated electrons,^{17–20} as well as characteristic features of metallic nanoparticles²¹ and semiconducting nanostructures.²² Nevertheless, spectroscopy in the THz frequency range continues to be a challenging undertaking. Experimental difficulties related to this task are epitomized in a common reference to the THz frequency interval as to a “gap” between microwave and infrared (IR) methods. Indeed, it is difficult to extend microwave methods beyond a couple of hundred gigahertz (GHz) and likewise the extension of IR methods below the usual boundary of 3 THz (100 cm^{-1}) is similarly complicated. The latter task is especially challenging when the studied materials are highly reflective and available only in the form of millimeter-sized samples.

Driven by the importance of the THz frequency interval, various research teams have made significant advances in conquering this largely unexplored territory. Perhaps the most innovative approach is the time domain THz spectroscopy (TDS) pioneered by Grishkovsky.²³ Here radiation is generated and detected using hertz dipoles: metal stripes with a narrow gap prepared on the surface of an amorphous semiconductor. A laser pulse creates photoconductive carriers in a semiconductor, thus activating the dipoles. The duration of the photocurrent is of the order of 1 ps and thus the dipole generates radiation in a frequency region 0.1–4 THz (3–120 cm^{-1}). This technique allows one to obtain the real and imaginary parts of the optical constants of a medium through which radiation propagates without the use of Kramers–Kronig (KK) analysis.²⁴ TDS is employed exclusively in transmission mode. Several groups employed semi-coherent submillimeter sources such as backward wave oscillators and far-IR lasers. The scope of the experimental information extracted from these measurements is dramatically enhanced through the use of Mach–Zehnder²⁵ or Fabry–Pérot²⁶ interferometer schemes permitting evaluation of the optical constants without KK analysis. Yet another approach is based on the use of synchrotron light sources instead of conventional black-body sources in Fourier transform spectrometers. This latter approach capitalizes on the superior brightness of synchrotron sources compared to mercury lamps in the THz region.²⁷ Synchrotron operation in the regime of “coherent” emission may be especially advantageous for spectroscopy in THz regime.²⁸

In this article we describe the design and implementation of a sub-THz spectrometer based on a Martin–Puplett (MP) interferometer which has allowed us to achieve convenient operations at frequencies as low as 200 GHz using laboratory

^{a)}Electronic mail: dbasov@physics.ucsd.edu

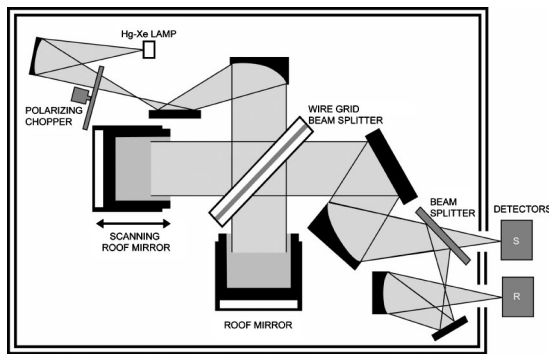


FIG. 1. Schematic diagram displaying the optical layout of a Martin-Puplett interferometer. Radiation is chopped with a rotating polarizer. The output polarizer also serves as a beam splitting element conveniently enabling a two-channel detection scheme. Optical components are assembled on an optical bread board located inside an evacuated compartment.

black body sources. Our research program is aimed at a systematic investigation of low temperature phase transitions of solids in the frequency domain. Particular interest is connected with the examination of the low energy electrodynamic of intermetallic superconductors, low dimensional electron gas, and heavy Fermion systems. All of these tasks demand that spectroscopic measurements are performed at temperatures below 1.5 K. Motivated by these latter considerations we have coupled a MP interferometer to a cryostat housing two independently controlled platforms cooled down with He-3. A combination of light pipe and focusing optics also housed in the same cryostat permits both transmission and absolute reflectance measurements with polarized light when the specimen temperature is as low as 340 mK. Apart from He-3 cryogenics which are uncommon in spectroscopic applications, we have developed an original two-channel signal detection scheme which is conveniently enabled by the optical layout of a MP interferometer. The two-channel detection has allowed us to minimize uncertainties in sub-THz measurements induced by relatively slow data acquisition of this step-scan instrument. We believe that this innovation may be useful in a variety of other applications of MP interferometers in particular for high resolution spectroscopy.

II. SYSTEM DESIGN AND COMPONENTS

A. Interferometer

The advantages of the interferometric approach to spectroscopy at infrared frequencies are firmly established.²⁹ Michelson interferometers are capable of providing unmatched spectral resolution and also superb signal stability. A serious disadvantage of Michelson interferometers is that beamsplitters (typically: mylar foils) are ineffective in the THz range. Following the original idea of Martin and Puplett³⁰ (MP) a wire grid polarizer can be used to obtain nearly perfect beamsplitter efficiency at frequencies as low as 20 GHz. MP interferometers are available through a number of vendors. The interferometer shown in Fig. 1 is based on a Sciencetech-200 instrument. The first elliptical mirror in the optical scheme collecting flux from a mercury-xenon lamp (Hamamatsu photonics L2482) has a numerical aper-

ture $f=2$. To preserve the f -number through the entire systems the beam-splitting wire grid polarizer has a diameter of 125 mm. We employed Al-wire polarizers deposited on a thin mylar substrate. The scanning roof mirror is positioned on an Aerotech ATS-803005U5 stage with total travel of 5 cm (split as 12.5 and 37.5 mm with respect to the zero path difference). The unapodized resolution of our instrument³¹ is $\delta=1/75 \text{ mm}^{-1}=450 \text{ MHz}$. All components of the interferometer are assembled on an optical breadboard and are housed in a vacuum compartment to avoid strong absorption in THz range at ambient conditions.

We have implemented several modifications to the standard MP scheme. In our setup the intensity of the THz beam is modulated by a rotating polarizer located in front of the first intermediate focus (Fig. 1); the fixed polarizer is positioned at the output of the interferometer. An obvious advantage of this configuration is that the output beam is linearly polarized. The output fixed polarizer is oriented approximately 45° with respect to the direction of the beam so that radiation exiting the interferometer is split into SAMPLE and REFERENCE channels. Note that the intensity in the reference channel is produced *without* reducing the signal level in the sample channel. Standard MP design implies that radiation reflected from the polarizer is “wasted” since no useful information is extracted from the analysis of this signal. In our scheme, we use the second channel to compensate for signal fluctuations and system drift in the course of the data acquisition process as will be described below. In the THz range, wire grid polarizers deliver very high beam-splitting efficiency and the signal level in both channels of our interferometer is approximately the same (see top panel of Fig. 5).

In Fig. 2 we show the power spectrum in the frequency region below 25 THz in one of the channels collected by means of a Si bolometer operating at 4.2 K. The upper frequency limit is imposed by a cutoff filter in the bolometer. The inset shows the interferogram recorded with a Stanford SR-850 lock-in amplifier. If perfect polarizers were employed within the MP scheme the intensity of the interferogram background away from the main peak would be vanishingly small so that $I_{\text{background}}/I_{\text{peak}}=0$. In practice, polarizers are not immune to minor leakage of unwanted polarization and $I_{\text{background}}/I_{\text{peak}}$ is always finite. We found that in our setup $I_{\text{background}}/I_{\text{peak}} < 1/20$ with detector cutoff at 25 THz (750 cm^{-1}) and $1/35$ – $1/50$ when the cutoff is at 1500 GHz (45 cm^{-1}). These “high contrast” interferograms produced by our interferometer is a testimony to the excellent efficiency of polarizers employed in the optical scheme. Another indicator of more than adequate polarizer performance is that the power spectrum (obtained by Fourier transforming the interferogram) shows significant signal levels even at $\omega > 15 \text{ THz}$ and is comparable to data generated by means of a Michelson interferometer working with a $3.5 \mu\text{m}$ mylar beamsplitter.

B. Dual platform He-3 cryostat

Interferometry-based spectroscopy of materials at low temperatures in the THz range requires the use of at least two

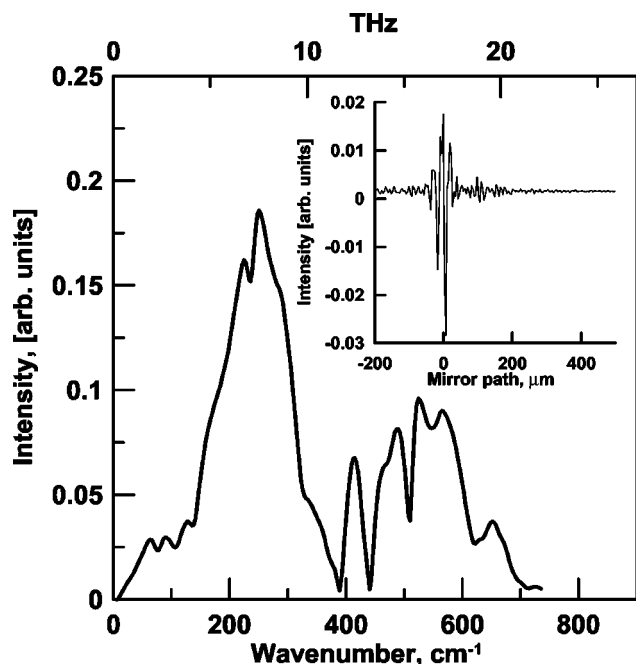


FIG. 2. Power spectrum produced by a Martin-Puplett interferometer and recorded using a Si bolometer operating at 4.2 K; resolution 4 cm^{-1} . Power spectra minima between $350\text{ and }550\text{ cm}^{-1}$ are triggered by absorption in the beam splitter. Inset shows a fragment of the double-sided interferogram (in the vicinity of the zero path difference) from which this power spectrum has been calculated.

cryogenic units: one for the studied specimen and the other for a He-cooled thermal (bolometric) detector. Usually separate cryostats are employed for these two essential units whereas focusing and polarizing optics components are located in an evacuated compartment of a spectrometer. We have chosen a different approach to the design of the cryogenic units for our sub-THz instrument (Fig. 3): two He-3 cold platforms (one for the sample and the other for detec-

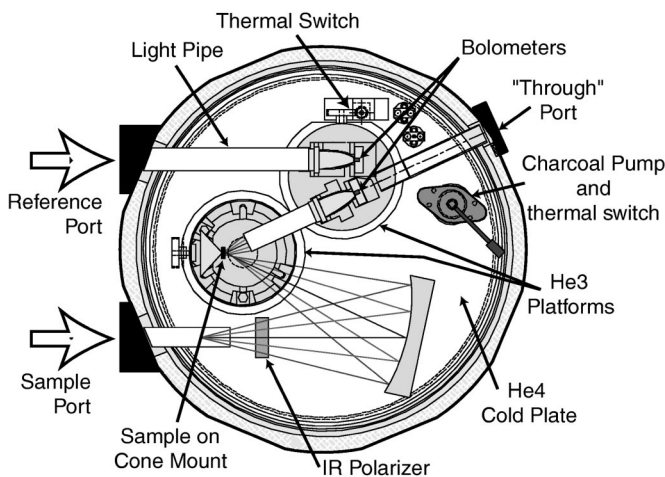


FIG. 3. Dual platform He-3 cryostat (bottom view). The cryostat is approximately 260 mm in diameter. The volume of the He-4 bath is approximately 6 l. He-3 storage containers (not shown) are attached to the cryostat. Thermal switches are operated using mechanical drives. Both the bottom plate of He-4 bath and bottom plates of He-3 platforms are fabricated in the form of optical breadboards to allow convenient rearrangement of optical components. The cryostat is presented in the optical layout for reflectance measurements.

tors) are located inside the *same* cryogenic unit. The focusing mirror and polarizer are attached to the bottom of a He-4 bath. This scheme has numerous advantages. In particular, the cryogenic system presented in Fig. 3 eliminates the need for additional sets of windows and cutoff filters that would be required if “sample” and “detector” cryostats had been decoupled. This cryostat has been fabricated based on our design at Infrared Laboratories, Tucson, Arizona. Similar cryogenics has been employed in a spectroscopic setup recently developed at Brock University.¹⁸ The operation of compact He-3 platforms using activated charcoal absorption pumps is described elsewhere.³² All the optical components and polarizer holders used in our system are built in house.

The cryostat is attached to the vacuum compartment of the MP interferometer. The entrance windows are made of quartz which is transparent below 3.5 THz. We use two sets of cutoff filters: one at the 77 K nitrogen-cooled shield and another attached to the He-4 cooled surface. We have chosen the upper cutoff to be at 1.5 THz (45 cm^{-1}) which makes an excellent overlap with the frequency range of a Michelson interferometer available in our laboratory: ($25\text{--}27\,000\text{ cm}^{-1}$). Incident beams coming from the interferometer are focused on the entrance of light pipes (ID=12.5 mm) installed directly behind the 77 K cutoff filters of the cryostat. The light pipe coupling allows us to minimize the diameter of the windows and filters without compromising the *f*-number of the system. Light pipes are fabricated from gold-plated electroformed nickel. The He-4 cooled cutoff filters are installed inside the light pipes. The light pipe in the reference channel guides radiation directly to the Winston cone of the reference detector. We employed doped Si bolometers made by Infrared Labs. Radiation in the sample channel is refocused using an elliptical mirror. Despite the fact that about 10 cm of the optical path occurs through the light pipe we obtain good image quality on the sample. The studied specimens are glued to a copper cone that is anchored to the cold surface of the sample He-3 platform. Only radiation reflected from the sample surface is directed towards the collecting light pipe that delivers the THz radiation to the Winston cone of the sample bolometer.

Temperature is monitored using Ge sensors (Lakeshore) directly at the bottom of the He-3 pot and at the top of the cone supporting studied specimens. Typical readings are 310 mK at the cold surface and 330–340 mK at the top of the cone. The duration of low temperature operation of He-3 platforms critically depends on details of a particular experiment. Operation at temperatures elevated compared the base $T=320\text{ mK}$ significantly compromises He-3 holding times. Temperature can be controlled either using a heater attached to He-3 platforms or by warming the charcoal pumps acting on the He-3 pots. If it is necessary to achieve temperatures above 1.7 K, the sample platform is linked to the He-4 bath of the cryostat using a mechanical thermal switch. We were able to reach temperatures up to 20–25 K on the sample platform while the detector platform is still kept at 320 mK. Typical He-3 holding times on the bolometer platform exceed 24 h with about 7.5 l of He-3 gas in our system. In order to achieve these reasonable holding times it was necessary to minimize radiation heating. We developed housings

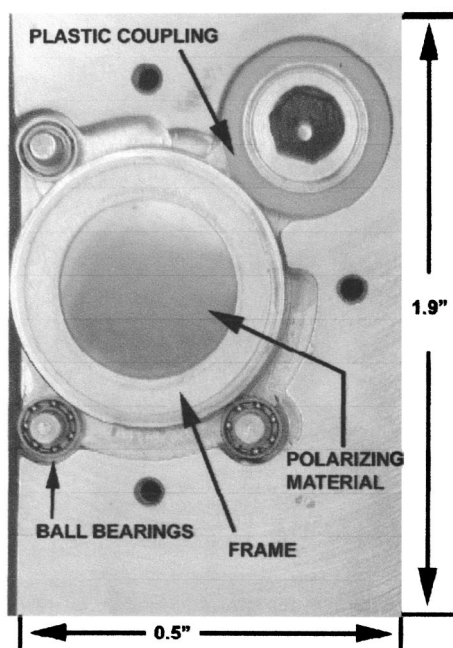


FIG. 4. A photograph of a custom made polarizer holder (with front cover taken off). The base plate is 0.5 in. \times 1.9 in. \times 1/4 in. supports a frame with a polarizing material. Frame can be rotated using a hexagonal knob. Side of the frame has markings every 5°.

that are thermally connected to the He-4 bath around each of the He-3 platforms. This prevents exposure of these platforms to surfaces warmer than 4.2 K (or 1.6 K under pumping). We were able to realize reliable operation of both He-3 platforms when the temperature of the He-4 bath is either 4.2 or 1.6 K (under pumping).

The cryostat shown in Fig. 3 is equipped with three infrared ports: sample, reference and through ports. This diagram depicts a system when it is arranged for reflectance measurements. Depending on the particular goals of the experiment the system can be easily reconfigured for other types of measurements. For instance, transmission experiments can be enabled by guiding radiation directly from the sample port to the sample bolometer (bypassing a refocusing mirror) with a studied specimen mounted on a sample platform. Alternatively, transmission measurements can be carried out using an optical layout shown in Fig. 9. The advantage of the latter approach is that the THz beam is focused on the sample surface permitting studies of smaller specimens without compromising signal intensity. The third port allows guiding of the THz beam through both He-3 platforms and is intended for spectroscopy with external detectors.

The light pipes employed to couple interferometer to the dual platform cryostat inevitably depolarize THz radiation. It is therefore imperative to employ a polarizer installed inside the cryostat for spectroscopic studies of anisotropic materials where linearly polarized light is required. The constrained space inside the cryostat rules out the use of bulky commercial polarizer holders. For this purpose we have developed an attachment shown in Fig. 4. A polarizer (Al wire grid on mylar substrate) is stretched on a frame supported by three ball bearings. The ID of the frame is 12.5 mm is identical to the ID of the light pipes. The side of the frame has markings

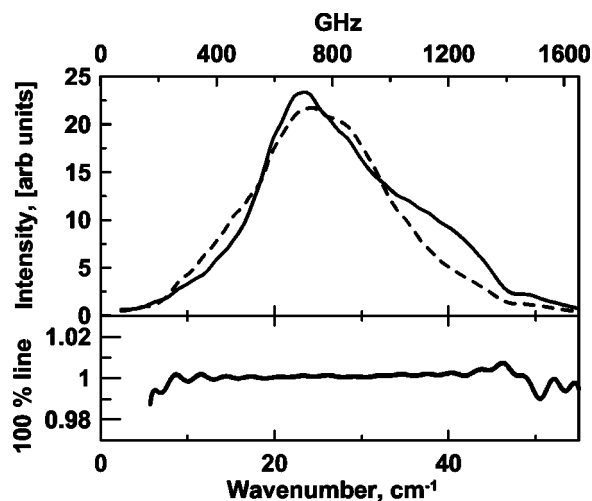


FIG. 5. Power spectra in the sample channel (solid line) and reference channel (dashed line) reveal approximately equal intensities when a large area stainless steel mirror is installed on the sample mount. Spectra are collected at $T=340$ mK with spectral resolution 1 cm^{-1} . The upper limit in the frequency scale is determined by cutoff filters. The bottom frame shows a 100% line obtained in the sample channel in two repetitive runs.

with a 5° step. The frame can be conveniently rotated using a plastic coupler also providing 2:1 gearing for accurate re-adjustment of the polarizer angle.

III. THz SPECTROSCOPY USING A MARTIN-PUPLETT INTERFEROMETER

A. The two-channel data acquisition mode

In Fig. 5 we show a typical power spectra collected using the cryostat depicted in Fig. 3. Both sample and reference channel data are presented. For the purpose of these measurements a large area stainless steel reflectance is mounted on the cone in the sample channel. The upper cutoff is determined by filtering optics. The power spectra are peaked at 800 GHz with intensity extending below 400 GHz. A standard performance characteristic of a spectrophotometric systems is the so-called 100% line: a ratio of two power spectra obtained in two repetitive runs under nominally identical condition. An examination of the 100% line displayed in the bottom frame of Fig. 5 indicates that our instrument permits acquisition of data down to nearly 200 GHz with good reproducibility and with the signal-to-noise ratio better than 1%.

In order to extract complete information about properties of a system through a spectroscopic experiment it is necessary to measure absolute values of experimentally accessible parameters: reflectance $R(\omega)$ and/or transmission $T(\omega)$. In the case of reflectance measurements this task requires that a studied specimen is replaced by a metallic mirror with known reflectivity. Then the sample reflectance is obtained by taking the ratio of the two signal intensities: $R(\omega) = I_{\text{sample}}(\omega)/I_{\text{mirror}}(\omega)$. This approach is generally realized through a mechanical repositioning of a sample so that it can be replaced by an identical mirror in the optical path. However, convenient mechanical schemes for switching between sample and reference cannot be employed when the sample is cooled down to He-3 temperatures. Instead, we used an

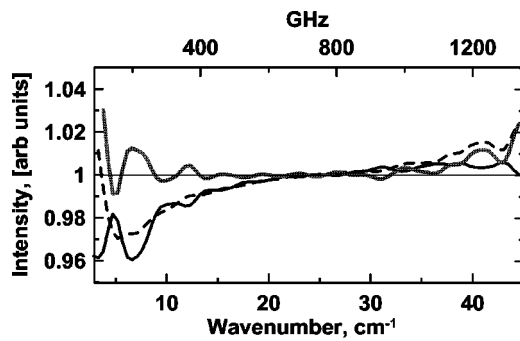


FIG. 6. Black lines: 100% lines in the sample (solid) and reference (dashed) channels measured approximately with the time interval of 20–30 min. Data collected with the spectral resolution 1 cm^{-1} . These spectra show systematic deviation of the base line from 1 that is particularly noticeable at $\omega < 700$ GHz. This systematic deviation is accounted for in the double-ratio spectrum (gray) which shows significant improvement of the baseline throughout the entire frequency range.

approach involving *in situ* coating of a sample with lead. Within this approach we first collect $I_{\text{sample}}(\omega)$ at various temperatures with simultaneous recording of the spectrum in the reference channel $I_{\text{reference}}(\omega)$. After a series of measurements is completed we coat the sample with approximately $1\text{--}2\ \mu\text{m}$ of lead and collect another full set of spectra $I_{\text{lead}}(\omega)$ again with simultaneous detection of the data in the reference channel. A *double ratio*: $[I_{\text{sample}}(\omega)/I_{\text{reference}}(\omega)]/[I_{\text{lead}}(\omega)/I_{\text{reference}}(\omega)]$ is then equivalent to $I_{\text{sample}}(\omega)/I_{\text{lead}}(\omega)$; the latter result can be used to obtain reflectivity of the studied material since reflectance of lead is known. Therefore, coating technique combined with two-channel data acquisition enables absolute measurements of $R(\omega)$ without need to mechanically reposition studied specimens.

The coating technique³³ when applied to more common spectroscopic investigations in infrared range delivers accurate results even in the case of microsamples.^{34,35} The reference signal is detected simultaneously with the signal reflected from the samples. Because sample and reference interferograms are collected during the *same* scan of the mirror the impact of system instabilities is minimized. When the instrument is operated at the highest possible resolution one scan may require 15–25 min or more. System drift is always present over such long periods of time; the role of the drift is also minimized by simultaneous data acquisition. This is exemplified in Fig. 6 where three 100% lines are displayed. Two of these lines were obtained by referencing two spectra generated in two sequential runs with a time difference of approximately 30 min. The other 100% line was obtained by taking a double ratio as described before. An improvement of the latter approach for the base line is clearly visible.

B. Reflectance and transmission measurements

In Fig. 7 we display the results of reflectance measurements for the superconductor $\text{La}_{1.875}\text{Sr}_{0.125}\text{CuO}_4$ carried out by means of our THz spectrometer (MP interferometer combined with the dual platform He-3 cryostat). Details of sample preparation and characterization were reported elsewhere.³⁶ Cuprate high- T_c superconductors are strongly

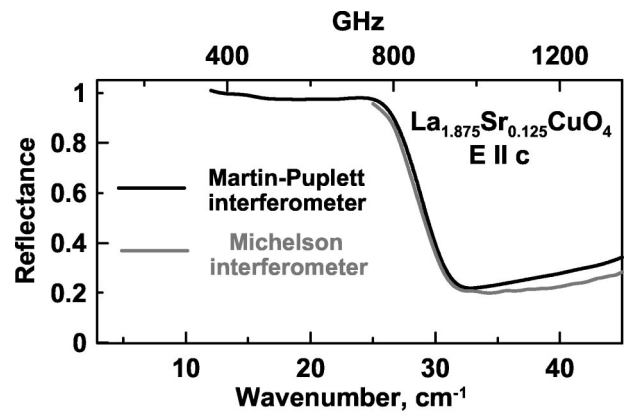


FIG. 7. Black line: reflectance spectrum of superconducting $\text{La}_{1.875}\text{Sr}_{0.125}\text{CuO}_4$ ($T_c = 32\text{ K}$) collected with the $E//c$ polarization at $T = 340\text{ mK}$ using the THz spectrometer presented in Figs. 1 and 3. Absolute value is obtained by *in situ* coating the studied specimen with Pb. Gray line: c -axis reflectance of the same sample measured at $T = 7.1\text{ K}$ using a Michelson interferometer available in our laboratory.

anisotropic with “metal-like” properties in the direction along the CuO_2 layers (ab plane of the crystal) coexisting with a nearly insulating response in the c -axis direction across the CuO_2 layers.³⁷ The dominant feature of the superconducting reflectance is a well-defined plasma edge. The absolute values of $R(\omega)$ approach 1 at the lowest energies; this region is followed by a sudden drop of reflectance forming an edge-like structure. At higher frequencies reflectance gradual recovers to the normal state value (close to 40% below 1 THz). The plasma edge is believed to originate from Josephson coupling between the CuO_2 planes and is often referred to as Josephson plasma resonance (JPR). One goal of the study reported in Fig. 7 was to resolve the frequency dependence associated with the JPR mode down to the lowest possible energies. The measurements have been performed on the ac -face of the crystal and required the use of linearly polarized light with $E//c$. In order to align the polarizer we have replaced the bolometric detector in the sample channel with a pyroelectric sensor and illuminated the entrance light pipe in this channel with a global source chopped at 110 Hz. The wire grid polarizer employed in this work delivers approximately 90% polarization efficiency at about 1500 cm^{-1} —the frequency range where the intensity of global source is peaked. The reflectance anisotropy of $\text{La}_{1.875}\text{Sr}_{0.125}\text{CuO}_4$ is largest in this frequency range. Therefore, the polarization dependence of the mid-IR signal measured with the lock-in and recorder with the step of 5° provided us with a reliable way to select the proper direction of the polarizing wire grid.

The absolute value of $R(\omega)$ in THz frequencies for $\text{La}_{1.875}\text{Sr}_{0.125}\text{CuO}_4$ crystal ($3.5 \times 3.5\text{ mm}^2$ on the ac face) shown in Fig. 7 was generated using the following procedure. We first measured $I_{\text{sample}}(\omega)$ simultaneously with $I_{\text{reference}}(\omega)$ in the course of several scans of the interferometer and then averaged ratios of the two signals to obtain $R'(\omega)$. We then coated the sample with Pb and measured $I_{\text{Pb}}(\omega)$ simultaneously with $I_{\text{reference}}(\omega)$. The ratios of the latter spectra also were averaged to produce $R''(\omega)$. Because reflectance of Pb is known (as will be discussed later), abso-

lute reflectivity of a studied specimen can be determined as $R(\omega) = R'(\omega)/R''(\omega)$. This procedure of double ratios allows us to collect sufficient data statistics in the process of repeated experiments and at the same time minimizes the impact of system long term drifts/instabilities. In Fig. 7 we also show the data for $\text{La}_{1.85}\text{Sr}_{0.125}\text{CuO}_4$ ($E//c$) generated with the Michelson interferometer equipped with a conventional 1.6 K bolometer. Limitations of both detector and beamsplitter employed in the latter experiment impose a cut-off close to 1 THz. This comparison also shows that the new instrument described in this work allows us to significantly extend the lower cutoff of spectroscopic measurements. We find a small discrepancy between the two spectra (up to 4% at the upper cutoff of the MP interferometer).

We used lead as a reference in our experiments for several reasons. The main advantage of Pb is that its $R(\omega)$ at $\omega < 800$ GHz is exactly 100%. Indeed, lead is a superconductor with $T_c = 7.1$ K and at $T \ll T_c$ its electrodynamic is in accord with Mattis–Bardeen theory prescribing $R(\omega) = 1$ for frequencies below the energy gap 2Δ ³⁸ (bottom panel of Fig. 8). Unity reflectance of Bardeen–Cooper–Schrieffer (BCS) superconductors has been experimentally verified through direct absorption measurements.³⁹ Moreover, lead can be conveniently coated atop of the studied specimens at low T unlike other commonly used reference metals including gold. The earlier circumstances make lead an “ideal” reference material for low temperature spectroscopy in sub-THz range. However, at frequencies above $2\Delta = 800$ GHz the reflectance of lead decreases. Because this drop of $R(\omega)$ occurs well within the energy range covered by our apparatus (Fig. 8) it is imperative to account for this deviation for an actual lead film used as a reference. Spectra calculated within the framework of the Mattis–Bardeen theory show that the amount by which reflectance decreases at $\omega > 2\Delta$ critically depends on the normal state resistivity ρ_{DC} . Therefore, accurate referencing of the data using Pb implies measurements of the resistivity of *in situ* grown films. This measurement is not complicated but requires knowledge of the thickness of the actual film. We found that it is more practical to characterize reflectance of lead reference using an alternative all-optics approach. The normal state reflectance of lead is adequately described with the Hagen–Rubens formula $R_n(\omega) = 1 - \sqrt{2\omega\rho_{DC}/\pi}$; at $T \ll T_c$ superconducting reflectance $R_s(\omega < 2\Delta) = 1$. Therefore, the R_s/R_n ratio at $\omega = 2\Delta$ allows us to estimate the magnitude of ρ_{DC} for the actual film obtained through *in situ* coating of studied specimens.

We have investigated a large number of thick Pb films grown both *in situ* and in a separate evaporation setup. Typical results are shown in the top panel of Fig. 8 where R_s/R_n spectra are plotted. This data set demonstrates that the sub-THz apparatus described here allows us to resolve small changes of reflectance well below 1% when sample dimensions do not exceed 3.5×3.5 mm². Within the signal-to-noise ratio of our experiment we find no temperature dependence between the R_s spectra taken at $T = 340$ mK and at $T = 2$ K; such changes are not expected for a superconductor with T_c as high as 7.1 K. The frequency dependence of $R_s(T = 340 \text{ mK})/R_n(T = 8 \text{ K})$ is peaked around 800 GHz which agrees well with the magnitude of the energy gap $2\Delta(0)$ in

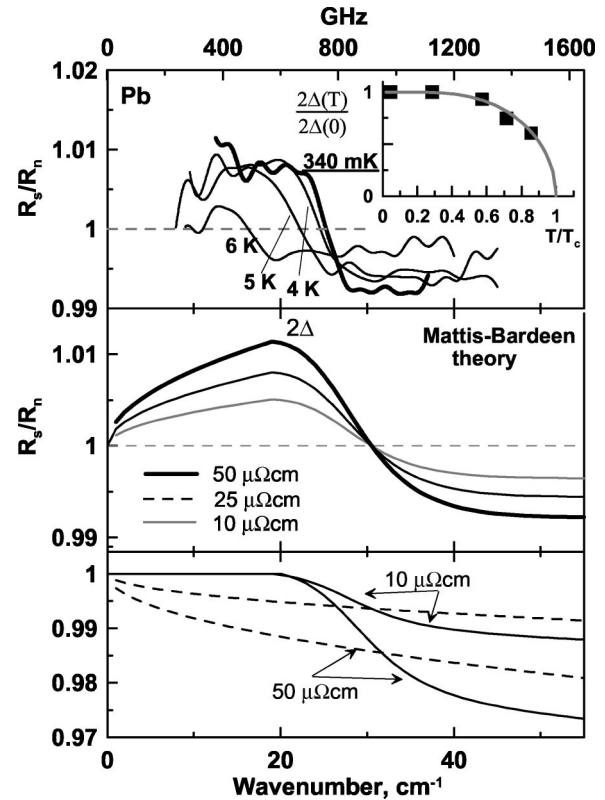


FIG. 8. Sub-THz reflectance of elemental superconductor Pb ($T_c = 7.1$ K). Top panel shows the ratios of reflectance in superconducting and normal state R_s/R_n . R_n was measured at 8 K for all spectra, R_s data were obtained at 340 mK (thick solid line), 4, 5, and 6 K (thin solid lines). In the vicinity of $\omega = 2\Delta(T)$ the R_s/R_n spectra show a broad maximum; above this frequency R_s/R_n decreases below 1. The magnitude of the energy gap at various T was extracted from the location of the edge in R_s/R_n and is depicted in the inset of the top panel. The middle panel shows R_s/R_n data generated using Mattis–Bardeen theory for $2\Delta = 21$ cm⁻¹ for various values of the normal state resistivity. The bottom frame displays absolute reflectivity of a BCS superconductor at $T \leq T_c$ (solid lines) and in the normal state (dashed lines) for two different values of the normal state resistivity ρ_{DC} .

bulk lead. The general form of the $R_s(T = 340 \text{ mK})/R_n(T = 8 \text{ K})$ spectrum is in fair agreement with the theoretical dependence shown in the middle frame of Fig. 8. We find a somewhat sharper increase of the experimental R_s/R_n close to the gap energy than in the theoretical dependence. Changes of the reflectance between 340 mK and 8 K are typically about 1% for a fairly disordered film. This latter value corresponds to the resistivity of the film about $\rho = 50$ $\mu\Omega$ cm which is characteristic for thick films grown at low temperatures. We also investigated the R_s/R_n ratios as a function of temperature. Selected spectra are displayed in the top panel of Fig. 8. We observe systematic decrease of the gap energy at finite T that is in good agreement with the BCS theory of superconductivity (inset of Fig. 8).

In addition to reflectance measurements we have carried out transmission studies of ultrathin Nb films on Si substrate. These films were grown at UIUC and had thickness of about 7.5 nm. The superconducting transition is suppressed in these ultrathin films down to 6 K.⁴⁰ For the purpose of these measurements we assembled the optical layout depicted in Fig. 9 permitting focusing THz radiation on the sample. In Fig. 10 we show the ratios of transmission measured at different

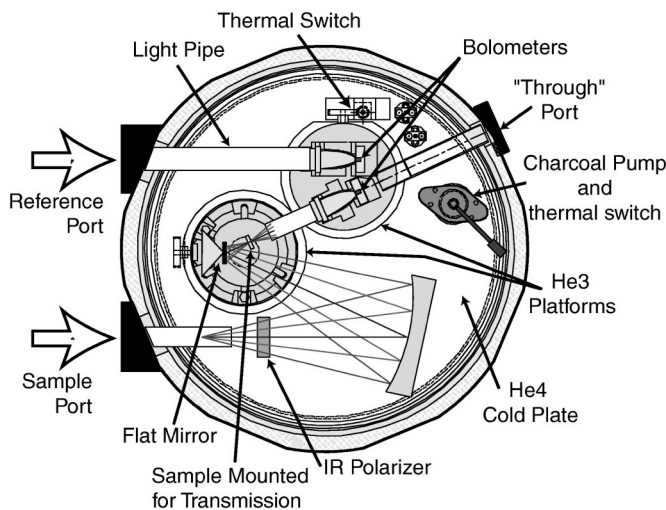


FIG. 9. Dual stage He-3 bolometer configured for transmission measurements. A large area flat mirror is now mounted on the cone. THz radiation in the sample channel is reflected from this mirror and is focused on a thin film sample.

temperatures in the superconducting state $T_s(\omega)$ to the data collected in the normal state at 8 K $T_n(\omega)$. Marked changes of transmission are related to the opening of the energy gap. The T_s/T_n spectra are peaked at frequencies close to the magnitude of 2Δ . This is also illustrated in the bottom frame of Fig. 10 where we show the T_s/T_n ratio calculated within the framework of Mattis–Bardeen model adequately describing electrodynamics of elemental superconductors in the dirty limit. Theoretical results are depicted for a free-

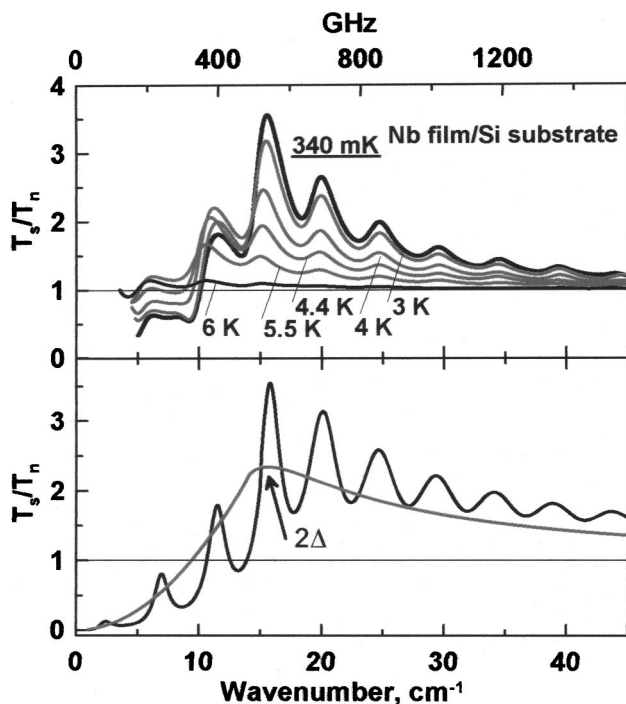


FIG. 10. Top panel: Transmission spectra T_s/T_n of Nb film on Si substrate ($T_c = 6$ K). T_s data were obtained at different temperatures between 340 mK and 6 K; T_n data were generated at 7 K for all spectra. Bottom panel: T_s/T_n spectra calculated within the Mattis–Bardeen theory with $2\Delta = 550$ GHz for a free standing film (gray line) and for a film on Si substrate (black line). Interference pattern occurs due to multiple reflections within the substrate.

standing film (gray line) and for a film on a Si substrate (black line). The latter result reveals a periodic pattern due to interference in the substrate. The value of the energy gap extracted from the fit is $2\Delta(T = 340 \text{ mK}) = 586 \text{ GHz}$ (17 cm^{-1}). This result corresponds to $2\Delta(0)/kT_c = 4.07$: a well established deviation from the weak-coupling predictions of the BCS theory: $2\Delta(0)/kT_c = 3.53$. Interestingly, the $2\Delta(0)/kT_c$ ratio in our ultrathin films does not seem to be affected by changes of T_c whereas the transition temperature itself is strongly reduced for film thickness below 90 Å. Recently, Pronin *et al.* have obtained $2\Delta(T = 4.5 \text{ K}) = 24 \text{ cm}^{-1}$ for a thicker 150 Å film with $T_c = 8.3 \text{ K}$ prepared using similar conditions.⁴¹ Their data corresponds to $2\Delta/kT_c$ close to 4.1 that is in excellent agreement with our findings. With increasing temperature the strength of the peak in the T_s/T_n data is reduced and the frequency position is shifted to lower energies. Both effects are in accord with the BCS theory.

ACKNOWLEDGMENTS

The authors are grateful to L. Carr, R. C. Dynes, C. C. Homes, T. Martin, M. Reedyk, T. Timusk, and M. Strongin for valuable discussion. Work at UCSD was funded by the NSF, DOE, and ONR. J.E. and L.H.G. acknowledge the U.S. Department of Energy, Division of Materials Sciences under Award No. DEFG02-ER9645439, through the Frederick Seitz Materials Research Laboratory, with Materials characterization carried out in the Center for Microanalysis of Materials, University of Illinois, which is partially supported by the U.S. Department of Energy under Grant No. DEFG02-91-ER45439.

- ¹N. I. Agladze, A. J. Sievers, S. A. Jones, J. M. Burlitch, and S. V. W. Beckwith, *Nature (London)* **372**, 243 (1994).
- ²J. W. Waters, *Proc. IEEE* **80**, 1679 (1992).
- ³R. A. Chevillat and D. Grischkowsky, *Appl. Phys. Lett.* **67**, 1960 (1995).
- ⁴V. M. Lubeke, K. Minzo, and G. M. Rebeiz, *IEEE Trans. Microwave Theory Tech.* **46**, 1821 (1998).
- ⁵D. M. Mittleman, R. H. Jacobsen, and M. C. Nuss, *IEEE J. Sel. Top. Quantum Electron.* **2**, 1077 (1996).
- ⁶J. O'Hara and D. Grischkowsky, *Opt. Lett.* **26**, 1918 (2001).
- ⁷Q. Wu, T. D. Hewitt, and X.-C. Zhang, *Appl. Phys. Lett.* **69**, 1026 (1996).
- ⁸For a prospective, see D. Cery, *Science* **297**, 761 (2002).
- ⁹A. J. Sievers, *J. Appl. Phys.* **41**, 980 (1970).
- ¹⁰For a recent overview, see *Handbook on Semiconductors*, edited by T. S. Moss and M. Balkanski (Elsevier, Amsterdam, 1994), Vol. 2.
- ¹¹A. J. Sievers, *Phys. Rev. Lett.* **13**, 310 (1964).
- ¹²D. N. Basov, T. Timusk, B. Dabrowski, and J. D. Jorgensen, *Phys. Rev. B* **50**, 3511 (1994); S. V. Dordevic, E. J. Singley, D. N. Basov, S. Komiya, Y. Ando, E. Bucher, C. C. Homes, and M. Strongin, *ibid.* **65**, 134511 (2002).
- ¹³P. L. Richards and M. Tinkham, *Phys. Rev. Lett.* **1**, 318 (1958).
- ¹⁴H. D. Drew and A. J. Sievers, *Phys. Rev. Lett.* **19**, 697 (1967).
- ¹⁵A. Mukhin, B. Gorshunov, M. Dressel, C. Sangregorio, and D. Gatteschi, *Phys. Rev. B* **63**, 214411 (2001).
- ¹⁶A. B. Sushkov, B. R. Jones, J. L. Musfeldt, Y. J. Wang, R. M. Achey, and N. S. Dalal, *Phys. Rev. B* **63**, 214408 (2001).
- ¹⁷M. Dressel, N. Kasper, K. Petukhov, D. N. Peligrad, B. Gorshunov, M. Jourdan, M. Huth, and H. Adrian, *Phys. Rev. B* **66**, 035110 (2002).
- ¹⁸M. G. Hildebrand, M. Reedyk, T. Katsufuji, and Y. Tokura, *Phys. Rev. Lett.* **87**, 227002 (2001).
- ¹⁹M. Grayson, L. B. Rigal, D. C. Schmadel, H. D. Drew, and P.-J. Kung, *Phys. Rev. Lett.* **89**, 037003 (2002).
- ²⁰J. Corson, J. Orenstein, S. Oh, J. O'Donnell, and J. N. Eckstein, *Phys. Rev. Lett.* **85**, 2569 (2000).

- ²¹D. B. Tanner, A. J. Sievers, and R. A. Buhrman, *Phys. Rev. B* **11**, 1330 (1975).
- ²²D. Heitmann and J. P. Kotthaus, *Phys. Today* **56** (1993).
- ²³D. Grishkovsky, S. Keiding, M. van Exter, and Ch. Fattinger, *J. Opt. Soc. Am.* **7**, 2006 (1990).
- ²⁴M. C. Nuss and J. Orenstein, in *Terahertz Time Domain Spectroscopy in Millimeter and Submillimeter Wave Spectroscopy of Solids*, edited by G. Gruner (Springer, Berlin, 1998).
- ²⁵B. P. Gorshunov *et al.*, *Int. J. Infrared Millimeter Waves* **14**, 683 (1993).
- ²⁶A. Schwartz, M. Dressel, A. Blank, T. Csiba, G. Grüner, A. A. Volkov, B. P. Gorshunov, and G. V. Kozlov, *Rev. Sci. Instrum.* **66**, 2943 (1995).
- ²⁷G. P. Williams, R. C. Budhani, C. J. Hirschmugl, G. L. Carr, S. Perkowitz, B. Lou, and T. R. Yang, *Phys. Rev. B* **41**, 4752 (1990).
- ²⁸G. L. Carr, M. C. Martin, W. R. McKinney, K. Jordan, G. R. Neil, and G. P. Williams, *Nature (London)* **420**, 153 (2002); M. Abo-Bakr, J. Feikes, K. Holldack, P. Kuske, W. B. Peatman, U. Schade, G. Wüstefeld, and H.-W. Hübers, *Phys. Rev. Lett.* **90**, 094801 (2003).
- ²⁹P. L. Richards, *J. Opt. Soc. Am.* **54**, 1474 (1964).
- ³⁰D. H. Martin and E. Puplett, *Infrared Phys.* **10**, 105 (1969).
- ³¹J. Chamberlain, *The Principles of Interferometric Spectroscopy* (Wiley, New York, 1979).
- ³²D. Walton, T. Timusk, and A. J. Sievers, *Rev. Sci. Instrum.* **42**, 1266 (1971).
- ³³C. C. Homes, M. A. Reedyk, D. A. Crandels, and T. Timusk, *Appl. Opt.* **32**, 2976 (1993).
- ³⁴D. N. Basov *et al.*, *Science* **283**, 49 (1999).
- ³⁵W. J. Padilla, D. N. Basov, and D. Mandrus, *Phys. Rev. B* **66**, 035120 (2002).
- ³⁶T. Suzuki *et al.*, *Phys. Rev. B* **57**, 3229 (1998).
- ³⁷For an overview see: D. N. Basov and T. Timusk, in *Handbook on the Physics and Chemistry of Rare Earths* (Elsevier Science, New York, 2001), Vol. 31, pp. 437–507.
- ³⁸D. C. Mattis and J. Bardeen, *Phys. Rev.* **111**, 412 (1958).
- ³⁹D. Miller *et al.*, *Phys. Rev. B* **47**, 8076 (1993).
- ⁴⁰I. V. Roshchin *et al.*, *Phys. Rev. B* **66**, 134530 (2002).
- ⁴¹A. V. Pronin, M. Dressel, A. Pimenov, A. Loidl, I. V. Roshchin, and L. H. Greene, *Phys. Rev. B* **57**, 14416 (1998).